AGU PUBLICATIONS

JGR

Journal of Geophysical Research: Solid Earth

RESEARCH ARTICLE
10.1002/2015JB011956

Key Points:
- The pore scale electrical environment of clays
- The connections between EM parameters and components of surface chemistry
- We measure the dispersion of the dielectic permittivity up to 160 GHz

Correspondence to:
R. Rahman,
rrahman@mines.edu

Citation:
Rahman, R., D. K. McCarty, and M. Prasad (2015), Sub-THz complex dielectric constants of smectite clay thin samples with Na^+/Ca^{++} ions, *J. Geophys. Res. Solid Earth*, *120*, 6219–6225, doi:10.1002/2015JB011956.

Received 19 FEB 2015
Accepted 30 JUL 2015
Accepted article online 4 AUG 2015
Published online 29 SEP 2015

Sub-THz complex dielectric constants of smectite clay thin samples with Na^+/Ca^{++} ions

Rezwanur Rahman[1,2,3], Douglas K. McCarty[4], and Manika Prasad[2,3]

[1]Department of Physics, Colorado School of Mines, Golden, Colorado, USA, [2]Department of Petroleum Engineering, Colorado School of Mines, Golden, Colorado, USA, [3]OCLASSH, Department of Petroleum Engineering, Colorado School of Mines, Golden, Colorado, USA, [4]Chevron ETC, Houston, Texas, USA

Abstract We implement a technique to characterize the electromagnetic properties at frequencies 100 to 165 GHz (3 cm^{-1} to 4.95 cm^{-1}) of oriented smectite samples using an open cavity resonator connected to a submillimeter wave VNA (Vector Network Analyzer). We measured dielectric constants perpendicular to the bedding plane on oriented Na^+ ion and Ca^{++} ion stabilized smectite samples deposited on a glass slide at ambient laboratory conditions (room temperature and room light). The clay layer is much thinner (~30 μm) than the glass substrate (~2.18 mm). The real part of dielectric constant, ϵ_{re}, is essentially constant over this frequency range but is larger in Na^+ ion than in Ca^{++} ion infused clay. The total electrical conductivity (associated with the imaginary part of dielectric constant, ϵ_{im}) of both samples increases monotonically at lower frequencies (<110 GHz) but shows rapid increase for Na^+ ions in the regime > 110 GHz. The dispersion of the samples display a dependence on the ionic strength in the clay interlayers, i.e., ζ potential in the Stern layers.

1. Introduction

Clay minerals have a complex layered structure with exchangeable cations that can bind water molecules in the interlayers. With increasing pressure and temperature, or in the presence of polar free radicals, these interlayer cations can be exchanged. This cation exchange capacity (CEC) of clay minerals affects their fluid conductivity [*Raythatha and Sen*, 1986] and permeability [*Raythatha and Sen*, 1986]; dielectric permittivity [*Chew and Sen*, 1982]. Complex dielectric properties of clay are crucial to determine hydrocarbon contents in oil-rich rocks. These measurements have been made predominantly at frequencies in the kilohertz range [*Mehran and Arulanandan*, 1977; *Chorom and Rengasamy*, 1995] and between 0.5 MHz and 1.1 GHz [*Raythatha and Sen*, 1986]. Complex conductivity of clayey materials between 1 mHz and 45 kHz has been modelled for CEC effects. *Revil et al.* [2013] and *Canan* [1999] researched dielectric properties of smectite clay samples in detail, explaining interlayer polarization and relaxation mechanisms between 30 kHz and 300 MHz. Some clay minerals can swell due to hydration with water adsorbed in the interlayer which depends on the charge of the interlayer cations and clay layer charge. Electrical measurements can yield cation mobility. Dielectric measurements can be instrumental to characterize the water absorbed in smectites [*Weiler and Chaussidon*, 1968]. The conductivities of smectite clays saturated by monovalent cations has also been studied in detail [*Calvet*, 1975; *Fripiat et al.*, 1965]. These frequency- and temperature-dependent measurements were in the frequency range between 300 Hz and 10 kHz, and from −150°C to +30°C. In a much higher-frequency domain, the THz dielectric constants of layered silicates including muscovite, vermiculite, phlogopite, and biotite have been measured by terahertz (THz)-time domain spectroscopy [*Janek et al.*, 2009]. Unfortunately, this technique is fairly noisy and low resolution since the THz pulses are very weak. So in this paper we look at monmorillionite using much higher-resolution CW methods based on harmonic multiplication of phase stabilized microwaves, electronically generated; these methods provide very low noise/high dynamic range out to about 1.4 THz at present.

2. Methods

At Colorado school of Mines (CSM) we use 3 mm wave (or sub-THz) modalities to extract material properties: (1) a quasioptical system, [*Scales and Batzle*, 2006b, 2006a; *Greeney and Scales*, 2012] to study bulk properties; (2) a near-field scanning system [*Weiss et al.*, 2009], to measure local properties; and (3) the open hemispherical

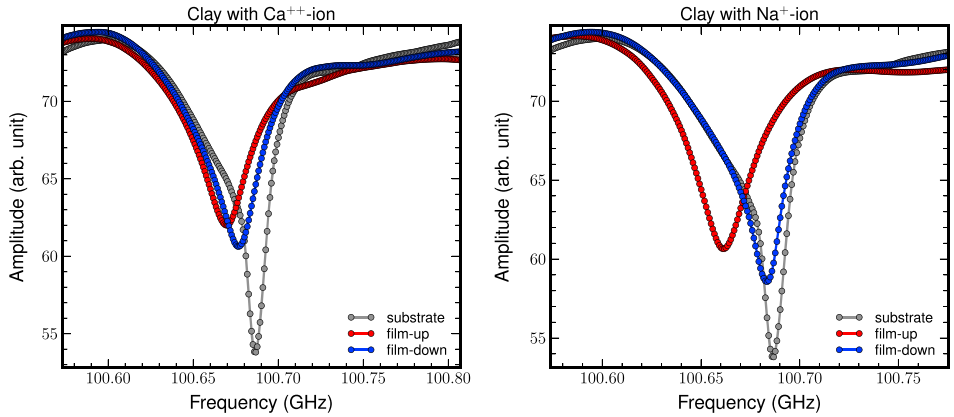

Figure 1. Perturbations with substrate only, film up, and film down setups for clay with (a) Ca^{++} and (b) Na^{+} ions (at room temperature).

cavity resonator [*Rahman et al.*, 2013; *Dudorov et al.*, 2005], for samples that are too thin or too low loss for quasioptical techniques. In this work, using cavity resonance perturbation (Figure 1), we extract the complex dielectric constants of clay-thin films in 100–165 GHz and investigate electrical properties in the presence of Ca^{++}/Na^{+} ions. We studied how these cations influence conductivity of free carriers and relaxations, and compare our data with low-frequency measurements [*Raythatha and Sen*, 1986].

We use an open hemispherical cavity resonator with VNA (Vector Network Analyzer) [*Rahman et al.*, 2013] to measure electrical properties of thin sections of clay samples exchanged with Ca^{++}/Na^{+} ions. The cavity is a structure with two copper mirrors positioned at certain distance (the "cavity length") without any sidewalls. The top mirror is hemispherical and connected to two WR-10 waveguide couplers working as a transmitter and a receiver, the lower mirror is flat and smaller than the upper one. We measured the real part of refractive index of ~1 mm thick glass substrate (borosillicate) to be 1.98 at 310 GHz which is the same as its published value [*Rahman et al.*, 2013]. For details on the cavity and methodology see *Rahman et al.* [2013].

2.1. Open Cavity Resonator

The principle of this technique is cavity perturbation. The changes in axisymmetric mode profiles, mainly the frequency shift and linewidth variation, between an empty cavity mode and the same mode in presence of a sample, allow us to determine the complex dielectric constant of the sample [*Cullen and Yu*, 1971; *Yu and Cullen*, 1982; *Hirovnen et al.*, 1996]. The unloaded (empty) cavity has an axisymmetric mode spacing that is $c/2L$, where L is the distance between two mirrors, also known as cavity length. In our cavity, since L is around 15 cm, the unloaded mode spacing is about 1 GHz.

Putting a sample on the bottom mirror perturbs the modes in a calculable but nontrivial way. To avoid geometrical factors, we do a second perturbation which involves flipping the sample upside down. Since the boundary values of the E field are different, we are able to get a simple (geometry-free) formula for the complex permittivity from three sweeps around a 00q mode. This complex dielectric permittivity is related to total electrical/optical conductivity and absorption coefficient [*Strom and Taylor*, 1977] with the use of basic theory of electromagnetism as

$$n_{re}\alpha = 120\pi\sigma_{re} = 30\omega\epsilon_{im}$$

where n_{re} and σ_{re} are the real part of the refractive index and conductivity (in $\Omega^{-1}\text{cm}^{-1}$), ϵ_{im} is imaginary part of the complex dielectric constant, and ω and α are frequency and absorption coefficient, respectively, expressed in terms of wave numbers (cm^{-1} relative to the speed of light), so 1 cm^{-1} corresponds to 30 GHz. The electrical conductivity is a macroscopic quantity which can be due to bound electrons (which is responsible for polarization and relaxation) or free electrons (which is Drude-type mechanism). This is also valid for absorption coefficient. These parameters, σ_{re} and α, essentially describe the loss mechanisms in a material.

2.2. Measurements

By sweeping the VNA, we identified the axisymetric empty cavity modes based on constant frequency spacing. This fixes the cavity length, L, to be 145.56 mm and kept it unchanged throughout the experiments.

Using a least squares fit of the data to a Breit-Wigner model (as described in *Rahman et al.* [2013]) we retrieve the eigenfrequency shifts and modal quality factors (Q values related to a linewidth) for substrate-only, film up and film down positions in order to apply the differential method. In order to determine uncertainty in the experiment, we repeat the entire procedure of inserting the sample, performing the measurements, and taking it out 6 times and calculating the variations in frequency shifts and linewidth changes of substrate. In *Rahman et al.* [2013] we showed that by redoing the entire procedure 6 times for borosillicate glass substrate, we obtained standard deviations less than 1.0% in the complex dielectric constant. This uncertainty also propagates to the calculations of dielectric constant. For consistency we confirmed during each trial that the same part of the samples is probed.

The frequency shifts due to film up, film down, and substrate only are used in equation (1) to determine the real part of the refractive index of a thin film [*Rahman et al.*, 2013; *Dudorov et al.*, 2005]. This is called the differential method since it involves measurements with the sample film up and down; the film will then see a different field because of the boundary conditions. The result is that sample geometry factors cancel out, greatly simplifying the calculation. Let n_f and n_s refer, respectively, to the refractive index of the film and substrate being measured. Then one can show that

$$\frac{\delta\nu_f}{\delta\nu_s} = \frac{n_f^2 - 1}{n_s^2 - 1}. \tag{1}$$

With

$$\delta\nu_f = \nu_{(\mathrm{fup})} - \nu_{(s)}. \tag{2}$$

$$\delta\nu_s = \nu_{(\mathrm{fdown})} - \nu_{(s)}. \tag{3}$$

Here $\nu_{(\mathrm{fup})}$, $\nu_{(\mathrm{fdown})}$, and $\nu_{(s)}$ represent the eigenfrequency associated with the film on the top (film up), film at the bottom (film down), and the substrate only, respectively. The term $\delta\nu_s$ stands for the difference between the eigenfrequencies associated with film at the bottom of the substrate and the substrate only, and the term $\delta\nu_f$ is the difference between the eigenfrequencies with the film at the top of substrate and the substrate only. The required condition is the real part of the refractive index of substrate must be known; or since the substrate is large enough, we can measure its permittivity directly using the quasi-optical methodology. The real part of the dielectric constant of thin film can obtained by $\epsilon_{re}^{(f)} = (\mathrm{n}_{re}^{(f)})^2$. We need Q values of film up and substrate (only) to calculate the imaginary part of complex dielectric constant of the thin film. The Q value of a resonant peak (perturbation) is defined as $\mathrm{Q} = \nu_0/\Delta\nu$. The Q value is related to the imaginary part of the refractive index by $\mathrm{n}_{im} = 1/2Q$, so for a thin film, $\mathrm{n}_{im}^{(f)} = 1/2Q^{(f)}$. The latter expressions assume that Q is not too small (say less than 10). In a cavity such as ours, the Q could be $10^4 - 10^5$ depending on technical details of the waveguide coupling. In the differential method, $Q^{(f)} = (Q^{(\mathrm{filmup})} - Q^{(\mathrm{substrate})})$. Now, we are able to compute the imaginary part of the complex dielectric constant of the thin film by

$$\epsilon_{im}^{(f)} = 2\mathrm{n}_{re}^{(f)}\mathrm{n}_{im}^{(f)}.$$

2.3. Samples and Sample Preparations

We studied smectite clay (SWy) from the Clay Minerals Society (||www.clays. org||) that were treated to yield homoionic, univalent (Na^+), and divalent (Ca^{++}) samples. The samples were treated to remove carbonate and iron oxide cements with a Na-acetate buffer and Na-dithionite, respectively *Jackson* [1985]. The sub-0.5 μm equivalent spherical diameter size fractions were separated from bulk samples by standard centrifuge methods. Then the Na^+ saturated clay was thoroughly cleaned with dialysis to remove excess salt. To prepare the Ca^{++} exchanged smectite, a dialyzed Na^+ sample was treated with a 1 M solution of $CaCl_2$, and shaken for at least two hours, excess solution was decanted and the process was repeated twice more. The excess Ca^{++} salt was removed with dialysis [*Moore and Reynolds*, 1997]. Oriented aggregates were made by evaporation onto glass slides to provide a sample ~4 cm long with at least 10 mg/cm^2 of clay [*Moore and Reynolds*, 1997]. This evaporation method yields deposition of clay particles on the glass slide with the clay layers parallel to the glass slide [*Prasad et al.*, 2002].

X-ray diffraction (XRD) measurements showed systematic differences between Na^+ smectite and Ca^{++} smectite. The structure of smectite determined from oriented aggregate sample preparations and X-ray diffraction (XRD) profile modeling and especially the interlayer water complex under different environmental conditions,

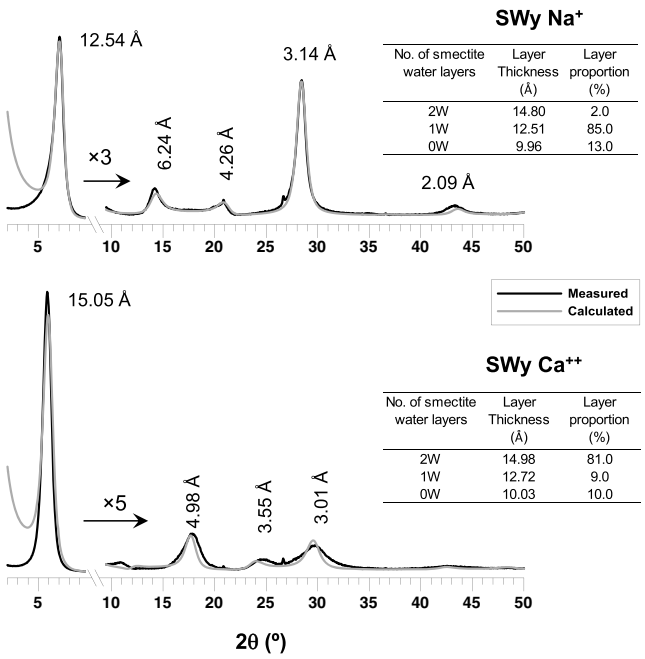

Figure 2. Experimental and simulated XRD patterns from oriented aggregate preparations from Ca^{++} ion and Na^{+} ion stabilized clay samples used in EM analysis.

is described in detail by *Ferrage et al.* [2005a, 2005b, 2010, 2011]. *Ferrage et al.* [2011] discuss the influence that the structure and organization of interlayer water has on the material's dielectric constant. For this reason, the diffraction profiles from the Na^{+} and Ca^{++} exchanged preparations used in the dielectric measurements in this study were simulated following the same methods as described by *Drits and Sakharov* [1976] and *Drits and Tchoubar* [1990]. The experimental and modeled diffraction patterns for the Na^{+} ion and Ca^{++} ion stabilized clay samples are shown in Figure 2 along with the thicknesses of bihydrated (2W), monohydrated (1W), and dehydrated (0W) layers and their proportions that were used in the simulated diffraction profiles. Under the ambient conditions of ~50% relative humidity (RH) in the laboratory the Na^{+} smectite is well described by random interstratifications of 2W (2%), 1W (85%), and 0W (13%). In contrast, the hydrated structure of Ca^{++} smectite was modeled by a different arrangement of layer thicknesses and proportions where 2W (81%), 1W (9%), and 0W (10%) were randomly interstratified. The XRD simulations in Figure 2 are not perfect with some misfit present at different angular ranges for the Ca^{++} and Na^{+} samples. This suggests that there is greater heterogeneity in the layer assemblage. However, the near perfect fit of the 001 reflection at 12.54 Å (Na) and 15.05 Å (Ca), and the generally good fit at higher angles indicate that the models represent the primary structures, with 1W layers being dominant in the Na^{+} sample and 2W layers being the dominant layer type in the Ca^{++} sample. Smectite interlayer water as probed by XRD, considered crystalline water [*Ferrage et al.*, 2011], may or may not all be coordinated to interlayer cations. Based on a combination of XRD and Grand-Canonical Monte Carlo simulations, *Ferrage et al.* [2011] found that fluctuations of charge locations and water dipoles affect the dielectric constant. These authors also point out that gravimetric adsorption methods produce similar but slightly higher molar equivalent water content than XRD experiments conducted under the same humidity conditions and based on the XRD simulation method. This is due to additional adsorption on surfaces and condensation in nanometer-scale pores.

Thus, in addition to millimeter wave electromagnetic (EM) analysis, we performed a variety of measurements on the two samples, including thermal gravimetric analysis, gravimetric water adsorption, and subcritical nitrogen gas adsorption to characterize physical differences that exist between the Na^{+} and Ca^{++} exchanged samples. Na^{+} smectite has higher specific surface area (SSA) and dominant 1–3 nm pores typical for clay aggregates; in contrast, the Ca^{++} smectite sample has predominantly larger pores between 50 and 100 nm [*Kuila et al.*, 2014]. At ~50 RH gravimetric water adsorption data (Figure 3) from SWy-Ca^{++} and SWy-Na^{+} showed that the Ca^{++} smectite adsorbed ~17.5 wt % following dehydration at 60°C for 3 h, compared to 10 wt % for the Na^{+} smectite under the same conditions. The hydration enthalpy is about 4 times greater

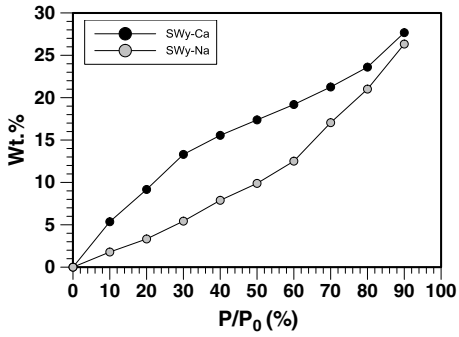

Figure 3. Gravimetric water adsorption isotherms for SWy-Ca and SWy-Na samples following drying at 60°C for 3 h.

for Ca^{++} than Na^{+} cations and is consistent with these gravimetric data. However, in the oriented aggregate preparations used for the EM analysis the contrasting structural arrangement of the interlayer crystalline water between the Na^{+} and Ca^{++} smectite samples (Figure 2) must play a significant role in the EM response [*Ferrage et al.*, 2011].

3. Results and Discussion

Referring to Figure 4, one can see that the real part of the dielectric constants of both clay samples are nearly dispersion free (i.e., frequency independent) in our range of measurements, indicating that carrier concentrations are low in both [*Zallen*, 1983; *Rahman et al.*, 2014]. The imaginary part of dielectric constant and electrical

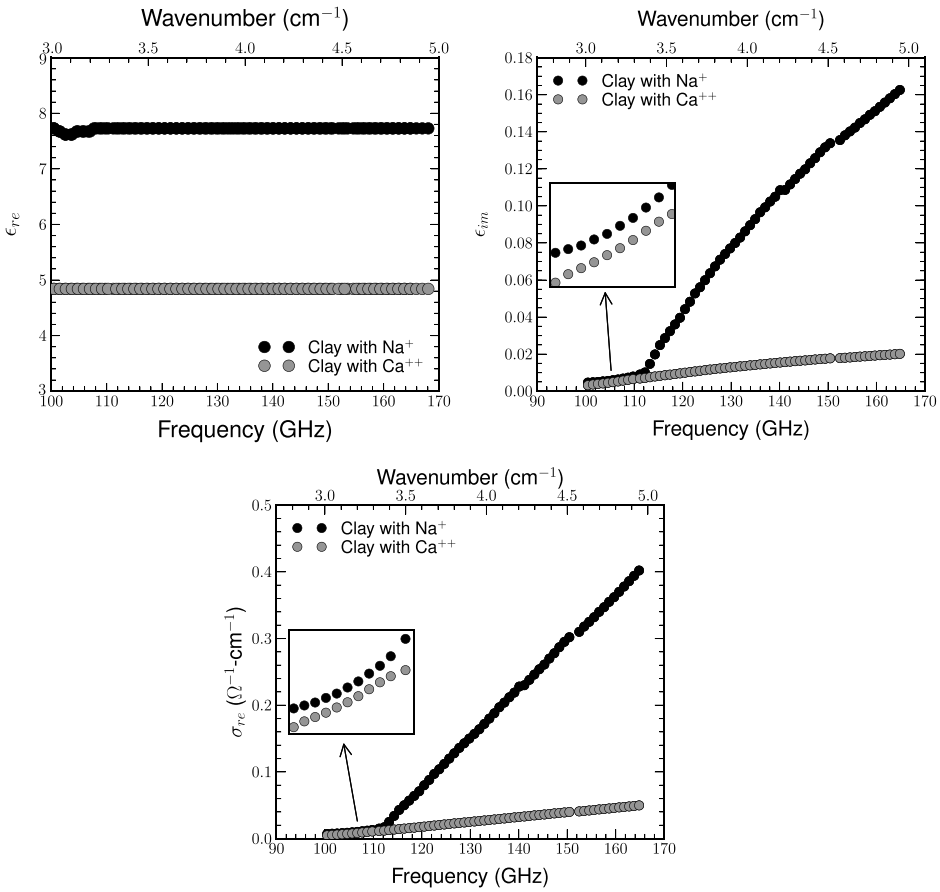

Figure 4. High-frequency (100–165 GHz) data of (top left) real part and (top right) imaginary part of the complex dielectric constants of clay samples with Na^{+}/Ca^{++} ions (at room temperature); (bottom) conductivity of both samples (inner plot is the expansion of the 100–110 GHz responses).

conductivity of the Na^+ exchanged sample increases at two different rates: faster in the higher-frequency range of our measurement and slower at low frequencies. The presence of both Debye relaxation [*Debye*, 1929] and Maxwell-Wagner relaxation [*Hamon*, 1953] at radio frequencies has been reported [*Calvet*, 1975]. But between 100 and 165 GHz, phonon-induced relaxation is dominant [*Zallen*, 1983].

Revil et al. [2013] proposed a theoretical model to study complex conductivity dependences on cation exchange capacity (CEC), (SSA), and salinity for clay samples at low frequency. This model also relates CEC to SSA with consistency [*Revil et al.*, 2013]. It is reported that SSA increases exponentially for Na^+ clay and linearly for Ca^{++} clay sample [*Egashira and Matsumoto*, 1981]. From our research, it is evident that conductivity depends on CEC or SSA. The larger CEC or exponential-growing SSA can contribute to more disperse Stern layer, and the smaller CEC or linearly progressive SSA stabilize the Stern layer. Thus, electrical conductivity is linked to CEC and zeta potential in the Stern layer [*Chorom and Rengasamy*, 1995]. The Na^+ makes a thicker unstable double layer where these high-mobility ions are able to polarize rapidly. Therefore, the conductivity is more dispersive. This interlayer polarization is correlated to relaxation mechanisms. The relaxation processes are, therefore, dependent of ζ potential which is also correlated to CEC [*Zadaka et al.*, 2010]. On the other hand, The imaginary part of dielectric constant and conductivity of the sample with Ca^{++} increases monotonically and sublinearly. The Ca^{++} creates more stable double Stern layer. Due to low mobility, the interlayer polarization is less disperse, so its conductivity is sublinear. Since $\epsilon_{im} = 2\,(1/\nu)\,\sigma_{re}$, the effect of $(1/\nu)$ is more into imaginary part of complex dielectric constant of samples with Na^{++} than that of Ca^{++}. In this case, ϵ_{im} at high frequencies faced steeper decrease than at lower frequency ends.

Comparing the results from *Raythatha and Sen* [1986] with ours (Figure 4), it is clear that in the sub-THz, the electrical conductivities of clay Na^+/Ca^{++} ions are almost 2 to 3 orders of magnitude greater than in the RF/microwave range. On the other hand, the real part of dielectric constants for both samples are roughly an order of magnitude larger in the RF/microwave range than in the sub-THz. The huge RF/microwave permittivities have been attributed to polarization of the double layer surrounding the ions [*Raythatha and Sen*, 1986]. The lower (and nearly frequency-independent) values of ϵ_{re} suggest that there are depletions of mobile charges due to phonon interactions causing the diffused layers to thin.

4. Conclusion

We measured sub-THz complex dielectric properties of clay samples with Na^+/Ca^{++} and compute their ϵ_{re} and σ_{re}. We illustrate the connections between electromagnetic parameters and components of surface chemistry such as CEC or SSA, ζ potential. This also enables us to study the clay content and free radicals in shales and to investigate their CEC and ζ potential dependences. In future, we will study different clay samples and exchange cations with broader frequency ranges to capture more complete frequency dependences of ϵ_{re} and ϵ_{im}. This will allow us to model computationally the dispersions of these parameters.

Acknowledgments

This work was supported by OCLASSH consortium and the US Department of Energy (Basic Energy Science) under grant DE-FG02-09ER16018. We thank John Scales for his insightful discussion on complex dielectric measurements. The Scales lab makes all of its data available, either on-line or by request, at no cost. This work is dedicated to the memory of Mike Batzle, who inspired us all.

References

Calvet, R. (1975), Dielectric properties of montmorillonites saturated by bivalent cations, *Clay Clay Miner.*, *23*, 257–265.

Canan, B. (1999), Dielectric properties of mixtures of clay-water-organic compounds, PhD thesis, Dept. of Geophys., Colo. School of Mines, Golden, Colo.

Chew, W. C., and P. N. Sen (1982), Potential of a sphere in an ionic solution in thin double-layer approximations, *J. Chem. Phys.*, *77*, 2042–2044.

Chorom, M., and P. Rengasamy (1995), Dispersion and zeta potential of pure clays as related to net particle charge under varying pH, electrolyte concentration and cation type, *Eur. J. Soil Sci.*, *46*, 657–665.

Cullen, A. L., and P. K. Yu (1971), The accurate measurement of permittivity by means of an open resonator, *Proc. R. Soc. London, Ser. A*, *325*, 49–71.

Debye, P. (1929), *Polar Molecules*, Chemical Catalogue Company, New York.

Drits, V., and B. Sakharov (1976), *X-ray Analysis of Mixed-Layer Clay Minerals*, Nauka, Moscow.

Drits, V., and C. Tchoubar (1990), *X-ray Diffraction by Disordered Lamellar Structures: Theory and Applications to Microdivided Silicates and Carbons*, Spring, Berlin.

Dudorov, S. N., D. V. Lioubtchenko, J. A. Mallat, and A. V. Raisanen (2005), Differential open resonator method for permittivity measurements of thin dielectric film on substrate, *IEEE Trans. Instrum. Measure.*, *54*, 1916–1920.

Egashira, K., and J. Matsumoto (1981), Relationship of the sediment volume of soil clays to surface area and mineralogical composition, *Soil Sci. Plant Nutr.*, *27*, 289–294.

Ferrage, E., B. Lanson, B. A. Sakharov, and V. A. Drits (2005a), Investigation of smectite hydration properties by modeling experimental X-ray diffraction patterns: Part I. Montmorillonite hydration properties, *Am. Mineral.*, *90*, 1358–1374.

Ferrage, E., B. Lanson, N. Malikova, A. Plançon, B. A. Sakharov, and V. A. Drits (2005b), New insights on the distribution of interlayer water in bi-hydrated smectite from X-ray diffraction profile modeling of 00l reflections, *Chem. Mater.*, *3499–3512*, 17.

Ferrage, E., B. Lanson, L. J. Michot, and J.-L. Robert (2010), Hydration properties and interlayer organization of water and ions in synthetic Na-smectite with tetrahedral layer charge. Part 1. Results from X-ray diffraction profile modeling, *J. Phys. Chem.*, *114*, 4515–4526.

Ferrage, E., et al. (2011), Hydration properties and interlayer organization of water and ions in synthetic Na-smectite with tetrahedral layer charge: Part 2. Toward a precise coupling between molecular simulations and diffraction data, *J. Phys. Chem.*, *115*, 1867–1881.
Fripiat, J. J., A. Jelli, G. Poncelet, and J. Andre (1965), Thermodynamic properties of adsorbed water molecules and electrical conduction in montmorillonites and silicas, *J. Phys. chem.*, *69*, 2185–2197.
Greeney, N. S., and J. A. Scales (2012), Non-contacting characterization of the electrical and mechanical properties of rocks at submillimeter scales, *Appl. Phys. Lett.*, *100*, 124,105, doi:10.1063/1.3692576.
Hamon, B. V. (1953), Maxwell-Wagner loss and absorption currents in dielectrics, *Aust. J. Phys.*, *6*, 304–315.
Hirovnen, M. T., P. Vainikainen, A. Lozowski, and A. V. Raisanen (1996), Measurement of dielectrics at 100 GHz with an open resonator connected to a network analyzer, *IEEE Trans. Instrum. Measure.*, *45*, 780–786.
Jackson, M. (1985), *Soil Chemical Analysis: Advanced Course*, 2nd ed., UW-Madison Libraries Parallel Press, Madison, Wis.
Janek, M., I. Bugár, D. Lorenc, V. Szöcs, D. Velič, and D. Chorvát (2009), Terahertz time-domain spectroscopy of selected layered silicates, *Clay Clay Miner.*, *57*, 416–424.
Kuila, U., D. McCarty, A. Derkowski, T. Fischer, T. Topór, and M. Prasad (2014), Nano-scale texture and porosity of organic matter and clay minerals in organic-rich mudrocks, *Fuel*, *135*, 359–373.
Mehran, M., and K. Arulanandan (1977), Low frequency conductivity dispersion in clay-water-electrolyte systems, *Clay Clay Miner.*, *25*, 39–48.
Moore, D., and R. J. Reynolds (1997), *X-ray Diffraction and the Identification and Analysis of Clay Minerals*, 2nd ed., Oxford Univ. Press, New York.
Prasad, M., M. Kopycinska, U. Rabe, and W. Arnold (2002), Measurement of Young's modulus of clay minerals using atomic force acoustic microscopy, *Geophys. Res. Lett.*, *29*(8), 1172, doi:10.1029/2001GL014054.
Rahman, R., P. C. Taylor, and J. A. Scales (2013), A system for measuring complex dielectric properties of thin films at submillimeter wavelengths using an open hemispherical cavity and a vector network analyzer, *Rev. Sci. Instrum.*, *84*, 83,901.
Rahman, R., T. R. Ohno, P. C. Taylor, and J. A. Scales (2014), Optically activated sub-millimeter dielectric relaxation in amorphous thin film silicon at room temperature, *Appl. Phys. Lett.*, *182,104*, 104, doi:10.1063/1.4874847.
Raythatha, R., and P. N. Sen (1986), Dielectric properties clay suspension in MHz to GHz range, *J. Colloid Interface Sci.*, *109*, 301–309.
Revil, A., J. Eppehimer, M. Skold, M. Karaoulis, L. Godinez, and M. Prasad (2013), Low-frequency complex conductivity of sandy and clayey materials, *J. Colloid Interface Sci.*, *398*, 193–209.
Scales, J. A., and M. Batzle (2006a), Millimeter wave spectroscopy of rocks and fluids, *Appl. Phys. Lett.*, *88*, 62,906, doi:10.1063/1.2172403.
Scales, J. A., and M. Batzle (2006b), Millimeter wave analysis of the dielectric properties of oil shales, *Appl. Phys. Lett.*, *89*, 24,102, doi:10.1063/1.2219720.
Strom, U., and P. C. Taylor (1977), Temperature and frequency dependences of the far-infrared and microwave optical absorption in amorphous materials, *Phys. Rev. B*, *16*, 5512, doi:10.1103/PhysRevB.16.5512.
Weiler, R. A., and J. Chaussidon (1968), Surface conductivity and dielectrical properties of montmorillonite gels, *Clay Clay Miner.*, *25*, 147–155.
Weiss, M., B. Zadler, S. Schafer, and J. A. Scales (2009), Near field millimeter wave microscopy with conical Teflon probes, *J. Appl. Phys.*, *106*, 4,902.
Yu, P. K., and A. L. Cullen (1982), Measurement of permittivity by Jeans of an open resonator: I. Theoretical, *Proc. R. Soc. London, Ser. A*, *380*, 49–71.
Zadaka, D., A. Radian, and Y. Mishael (2010), Applying zeta potential measurements to characterize the adsorption on montmorillonite of organic cations as monomers, micelles, or polymers, *J. Colloid Interface Sci.*, *352*, 171–177.
Zallen, R. (1983), *The Physics of Amorphous Solids*, Wiley-Interscience, New York.